JOURNAL OF GUIDANCE, CONTROL, AND DYNAMICS
Vol. 18, No. 6, November–December 1995

Resonance Capture in Unbalanced Dual-Spin Spacecraft

Raymond Tsui* and Christopher D. Hall†
U.S. Air Force Institute of Technology, Wright–Patterson Air Force Base, Ohio 45433

Spin-up dynamics of unbalanced dual-spin spacecraft may lead to a condition in which the spacecraft rotates in a nearly flat spin motion, transverse to the nominal spin axis. This condition has been described as a resonance trap, as precession phase lock, as stall, and as resonance capture. This phenomenon depends on spacecraft geometry, spin-up torque magnitude, and initial conditions. In this paper, we develop the concept of a probability of capture and construct a simple graphical tool that is used to illustrate sets of initial conditions that are likely to lead to capture.

Introduction

A DUAL-SPIN spacecraft consists of an inertially fixed or slowly spinning platform connected to a rotor that spins relatively fast to provide attitude stability. The classical gyrostat model has a balanced axisymmetric rotor coupled to a platform that may be unbalanced or asymmetric. Both bodies are rigid and are connected by a rigid shaft about which relative spin may occur, driven by either a constant-speed or constant-torque motor. The shaft is aligned with the rotor's axis of symmetry so that the moment of inertia tensor of the spacecraft is constant.

Spin-up of unbalanced or asymmetric dual-spin spacecraft may lead to undesirable tumbling motions. One way this can occur is through energy dissipation. An example of this was described by Scher and Farrenkopf[1] as the minimum energy trap, in which viscous damping along the spin axis causes the relative spin to diminish. Another kind of trap state they identified is the resonance trap, called precession phase lock (PPL) by Kinsey[2] and Kinsey et al.,[3] called stall by Or,[4] and identified as a type of resonance capture by Hall.[5]

Kinsey[2] and Kinsey et al.[3] defined PPL in terms of the angular velocities of the platform and rotor during spin-up. If the motor torque is too small, then once the unbalanced rotor reaches the spacecraft inertial free precession rate, the rotor velocity fails to maintain its steady increase. Instead, it decreases and the spacecraft's nutation angle grows. At the conclusion of this maneuver, the spacecraft tumbles in a flat spin about an axis transverse to the desired spin axis. During normal spin-up the rotor velocity exceeds the inertial free precession rate and continues to grow until the spin-up motor is deactivated, with a small net increase in nutation. It should be noted that the analysis of Kinsey[2] and Kinsey et al.,[3] is limited to dual-spin spacecraft with small unbalance. Likewise, the development in Or[4] is based on linearized equations assuming small nutation angles.

Hall examined resonance capture for gyrostats with asymmetric, balanced rotor[5] and gave a partial treatment for the asymmetric, unbalanced rotor case.[6] He established criteria for capture in terms of the system energy[5] and showed that nutation growth begins when trajectories of the perturbed system cross the instantaneous separatrices of the unperturbed system and is actually independent of the inertial free precession rate. He also established that resonance capture may be understood as a probabilistic phenomenon, dependent on initial conditions as well as on spacecraft geometry.

The initial conditions for a spin-up trajectory may be expressed in terms of three system variables: the platform axial angular momentum μ, and the system energy H, both of which are constant for zero spin-up torque, and a rapidly varying phase angle ϕ. Suppose a spin-up trajectory begins with known initial values of μ and H. It is reasonable to suppose that the exact initial value of the rapidly varying phase would be more difficult to determine precisely. Thus it is useful to know how the spin-up maneuver proceeds for all initial values of the phase angle ϕ. As shown herein, some initial values of ϕ lead to resonance capture, whereas others lead to the desired final dual-spin condition. Thus we develop the concept of a probability of capture for given initial conditions on μ and H.

In this paper, resonance capture is examined for the unbalanced gyrostat similar to the model studied by Kinsey[2] and Kinsey et al.,[3] but using quantitative capture criteria analogous to those developed in Ref. 5. A simple graphical tool is developed for depicting the probability of capture for a given spacecraft geometry and spin-up torque.

Equations of Motion

The model examined here is based on the gyrostat of Kinsey[2] and Kinsey et al.[3] as shown in Fig. 1. It differs from the classical system described earlier in that the platform ($\mathcal{P}$) is the balanced, axisymmetric body and the rotor ($\mathcal{R}$) is unbalanced. The rotor imbalance is limited to the $\hat{p}_1\hat{p}_3$ plane, where $\{\hat{p}_1, \hat{p}_2, \hat{p}_3\}$ is a pseudoprincipal reference frame. As described in Tsui,[7] this is a principal frame of the apparent gyrostat.[8] The spin-up motor torque is assumed to be a small constant, which is negative since the momentum of the platform is to be reduced to zero in the spin-up maneuver. We do not limit the analysis to slightly unbalanced systems, nor do we linearize about an equilibrium. Thus the approach developed herein applies to the general motion of a spacecraft with an arbitrary imbalance in

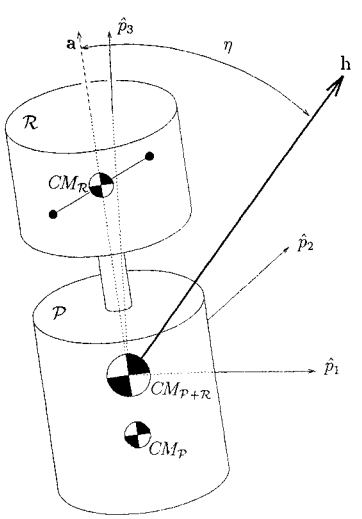

Fig. 1 Unbalanced gyrostat with rotor imbalance denoted by point masses.

Received May 20, 1994; presented as Paper 94-3714 at the AIAA/AAS Astrodynamics Conference, Scottsdale, AZ, Aug. 1–3, 1994; revision received March 20, 1995; accepted for publication March 21, 1995.

*Graduate Student, Astronautical Engineering; currently Captain, Titan Launch Facility Engineer, Cape Canaveral Air Force Base, FL 32925.

†Assistant Professor of Aerospace and Systems Engineering. Senior Member AIAA.

the $\hat{p}_1\hat{p}_3$ plane. Although we do assume small spin-up torque, the effect of its magnitude is also discussed and illustrated.

Because of the rotor imbalance, the governing equations are simpler when expressed in the frame in which $\boldsymbol{I} - I_s\boldsymbol{a}\boldsymbol{a}^T$ is diagonal, termed the pseudoprincipal frame. Here $\boldsymbol{I}$ is the moment of inertia tensor for the gyrostat, I_s is the axial moment of inertia of the platform, and $\boldsymbol{a}$ is the axis of relative rotation and symmetry axis of the platform. The system angular momentum vector $\boldsymbol{h}$ and the unit vector $\boldsymbol{a}$ are expressed in terms of their components in the pseudoprincipal frame. The rotational equations for torque-free motion are

$$\frac{dh_1}{d\tilde{t}} = h_2h_3\left(\frac{J_2 - J_3}{J_2J_3}\right) - \frac{h_2h_aa_3}{J_3} \tag{1}$$

$$\frac{dh_2}{d\tilde{t}} = h_1h_3\left(\frac{J_3 - J_1}{J_1J_3}\right) + \frac{h_1h_aa_3}{J_3} - \frac{h_3h_aa_1}{J_1} \tag{2}$$

$$\frac{dh_3}{d\tilde{t}} = h_1h_2\left(\frac{J_1 - J_2}{J_1J_2}\right) + \frac{h_2h_aa_1}{J_1} \tag{3}$$

$$\frac{dh_a}{d\tilde{t}} = g_a \tag{4}$$

where

g_a = torque applied by $\mathcal{R}$ on $\mathcal{P}$ about $\boldsymbol{a}$
h_a = angular momentum of $\mathcal{P}$ about $\boldsymbol{a}$
J_i = eigenvalues of $\boldsymbol{J} = \boldsymbol{I} - I_s\boldsymbol{a}\boldsymbol{a}^T$
$\tilde{t}$ = time
η = nutation angle, $\cos^{-1}(\boldsymbol{h}^T\boldsymbol{a}/\|\boldsymbol{h}\|)$

It should be noted that the angular velocity components are related to the angular momentum components by $\omega_i = (h_i - h_aa_i)/J_i$.

Nondimensionalizing these expressions simplifies the analysis further. First we define dimensionless inertia parameters as

$$i_1 = 1 - \frac{J_3}{J_1} \Rightarrow J_1 = \frac{J_3}{1 - i_1} \tag{5}$$

$$i_2 = 1 - \frac{J_3}{J_2} \Rightarrow J_2 = \frac{J_3}{1 - i_2} \tag{6}$$

$$i_3 = 1 - \frac{J_3}{J_3'} \Rightarrow J_3' = \frac{J_3}{1 - i_3} \Rightarrow i_3 = \frac{I_sa_3^2}{J_3'} \tag{7}$$

where $J_3' = J_3 + I_sa_3^2$. The dimensionless momentum components are defined as

$$x_i = h_i/h \qquad i = 1, 2, 3 \tag{8}$$

$$\mu = h_a/h \tag{9}$$

where $h = \|\boldsymbol{h}\|$, which is constant since there are no external torques. The dimensionless time and spin-up torque are defined as

$$t = \frac{h\tilde{t}}{J_3} \tag{10}$$

$$\varepsilon = \frac{g_aJ_3}{h^2} \tag{11}$$

Substitution of these definitions into Eqs. (1–4) produces four dimensionless equations of motion:

$$\dot{x}_1 = (i_2x_3 - \mu a_3)x_2 \tag{12}$$

$$\dot{x}_2 = -i_1x_1x_3 + \mu[a_3x_1 - a_1(1 - i_1)x_3] \tag{13}$$

$$\dot{x}_3 = [(i_1 - i_2)x_1 + (1 - i_1)\mu a_1]x_2 \tag{14}$$

$$\dot{\mu} = \varepsilon \tag{15}$$

where $\dot{(\,)} = d(\,)/dt$.

Conservation of angular momentum gives the integral

$$x_1^2 + x_2^2 + x_3^2 = 1 \tag{16}$$

which restricts solutions to a unit momentum sphere. From Eq. (15), we see that zero motor torque ($\varepsilon = 0$) corresponds to the condition $\mu = \text{const}$. In addition, rotational kinetic energy is conserved for $\varepsilon = 0$ and may be expressed as

$$T = \frac{1}{2}\left[\frac{(h_1 - h_aa_1)^2}{J_1} + \frac{h_2^2}{J_2} + \frac{(h_3 - h_aa_3)^2}{J_3} + \frac{h_a^2}{I_s}\right] \tag{17}$$

It is convenient to define a dimensionless energylike quantity H by

$$H = \frac{2J_3T}{h^2} - \mu^2\left(1 - i_1a_1^2 + \frac{1 - i_3}{i_3}a_3^2\right) \tag{18}$$

$$= 2\mu[(i_1 - 1)a_1x_1 - a_3x_3] - \left(i_1x_1^2 + i_2x_2^2\right) \tag{19}$$

It can be shown that H is a Hamiltonian for the system.[12] That is, Eqs. (12–14) may be written as a noncanonical Hamiltonian system in the form $\dot{\boldsymbol{x}} = (\frac{1}{2})\boldsymbol{x}^x\nabla H$, where $\boldsymbol{x} = (x_1, x_2, x_3)$, ∇H is the gradient of the Hamiltonian with respect to $\boldsymbol{x}$, and $\boldsymbol{x}^x$ is the skew symmetric matrix associated with the vector $\boldsymbol{x}$. We do not exploit the Hamiltonian nature of this problem in this paper, and the reader is referred to Ref. 12 for further details.

The system is integrable when $\varepsilon = 0$, but exact analytical solutions involve elliptic integrals and are not as tractable as in the axial case.[11] It is easy to see that most solutions are periodic functions of time, the exceptions being the separatrices connecting the saddle points. When $\varepsilon \neq 0$, the system does not admit closed-form solutions, and μ and H are not constant. The energy satisfies the differential equation

$$\dot{H} = 2\varepsilon[(i_1 - 1)a_1x_1 - a_3x_3] \tag{20}$$

Thus if $|\varepsilon| \ll 1$, then μ and H are slowly varying, and as shown in Refs. 11 and 12, one can study the slow flow of H vs μ. This is the approach taken here. All results are based on "exact" numerical solutions to the equations of motion, for a gyrostat with $i_1 = 0.7$, $i_2 = 0.3$, $i_3 = 0.8$, $a_1 = \frac{1}{2}$, and $a_3 = \sqrt{3}/2$. Note that $a_2 = 0$, since the rotor imbalance is assumed to be in the $\hat{p}_1\hat{p}_3$ plane.

Graphical Representations

For zero spin-up torque, the two constants associated with conservation of angular momentum [Eq. (16)] and conservation of energy [Eq. (19)] may be used to construct constant energy curves on a momentum sphere. This approach is well known and has been thoroughly explained in Hughes.[8] Spin-up maneuvers have been investigated using the momentum sphere approach by Barba and Aubrun[9] and Hubert.[10] One fundamental fact regarding Eqs. (12–14) and the $\varepsilon = 0$ momentum spheres is that there are either two, four, or six equilibrium points depending on the constant value of μ. The equilibria are either centers or saddles, similar to the steady spins of a rigid body about its principal axes. The curves passing through the saddles are called separatrices since they separate the regions of periodic orbits surrounding the centers. The separatrices are also trajectories with infinite period, each approaching a saddle as $t \to \infty$.

Example momentum spheres are shown in Figs. 2–4, for three different values of μ, illustrating the three different possibilities. In Fig. 2, where $\mu = 0.1$, there are six equilibria. Two of them correspond to steady spins close to the $\hat{p}_3$ axis. These are the desired oblate and prolate dual-spin conditions, denoted O_μ and P_μ, respectively. Two correspond to the two possible transverse spin configurations ($T_{1\mu}$ and $T_{2\mu}$) that may result from resonance capture. These four equilibria are stable. The two remaining equilibria are both unstable saddles (U_μ). The notation used here (O_μ, P_μ, $T_{1\mu}$, $T_{2\mu}$ U_μ) is similar to that developed in Refs. 11 and 12 and is a shorthand for the equilibrium components of the angular momentum vector. The subscript μ denotes the fact that the equilibria depend on the constant value of μ. For example, when $\mu = 0$, $O_\mu = (0, 0, -1)$ and $P_\mu = (0, 0, 1)$.

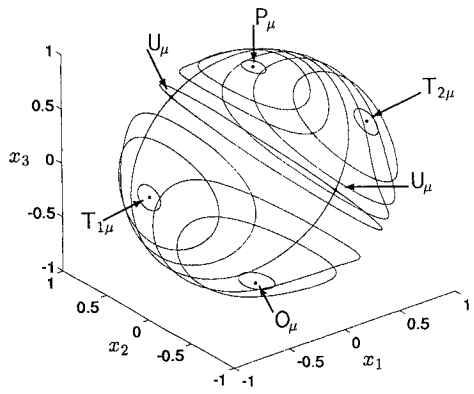

Fig. 2 Momentum sphere for $\mu = 0.1$.

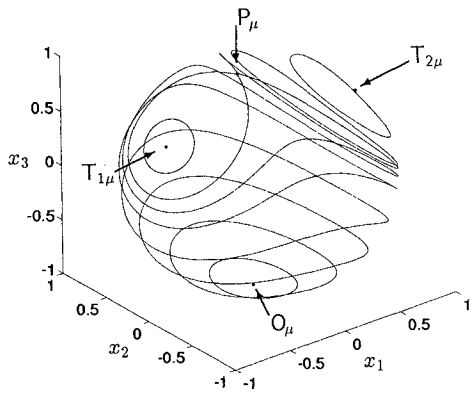

Fig. 3 Momentum sphere for $\mu = 0.4$.

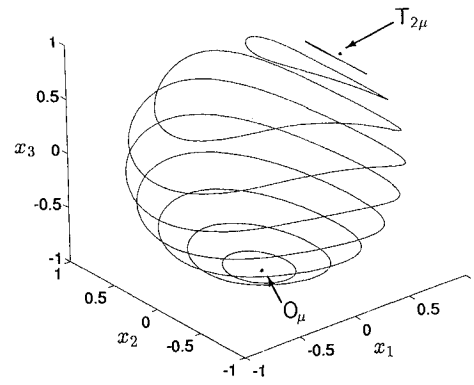

Fig. 4 Momentum sphere for $\mu = 0.7$.

In Fig. 3, where $\mu = 0.4$, there are four equilibria. Thus for a value of μ between 0.1 and 0.4, a bifurcation occurs. The bifurcation is in fact a pitchfork bifurcation where the center P_μ and the two saddles U_μ coalesce into a single saddle point. This is similar to the pitchfork bifurcations that occur for axial gyrostats.[11] The value of μ where this pitchfork occurs can be computed explicitly by noting that the saddle equilibria (U_μ) are at $(x_1, x_2, x_3) = [\mu a_1(i_1 - 1)/(i_1 - i_2), x_{2e}, \mu a_3/i_2]$. Conservation of angular momentum [Eq. (16)] then gives the two values of x_{2e}:

$$x_{2e} = \pm\sqrt{1 - \left(\frac{i_1 - 1}{i_1 - i_2}\right)^2 \mu^2 a_1^2 - \frac{\mu^2 a_3^2}{i_2^2}} \tag{21}$$

Thus real solutions only exist when $|\mu|$ is less than a certain value. This value, denoted μ_{pf}, is where the pitchfork occurs:

$$\mu_{pf} = \left\{\left[\frac{a_1(i_1 - 1)}{i_1 - i_2}\right]^2 + \left[\frac{a_3}{i_2}\right]^2\right\}^{-\frac{1}{2}} \tag{22}$$

In Fig. 4, where $\mu = 0.7$, there are only two equilibria. For a value of μ between 0.4 and 0.7 another bifurcation occurs. This bifurcation is a saddle-node bifurcation, or turning point, in which the saddle P_μ and the center $T_{1\mu}$ coalesce and disappear. Calculation of the value of μ for this bifurcation involves solving a quartic and is done numerically rather than analytically. The value of μ at this bifurcation point is denoted μ_{sn}.

Table 1 Classification of spacecraft geometry in terms of inertia parameters

	Requirement	
Classification	Dimensional	Dimensionless
Oblate-prolate	$J_1 > J_2 > J_3$	$i_1 > i_2 > 0$
Oblate-intermediate	$J_1 > J_3 > J_2$	$i_1 > 0 > i_2$
Intermediate-prolate	$J_2 > J_1 > J_3$	$i_2 > i_1 > 0$

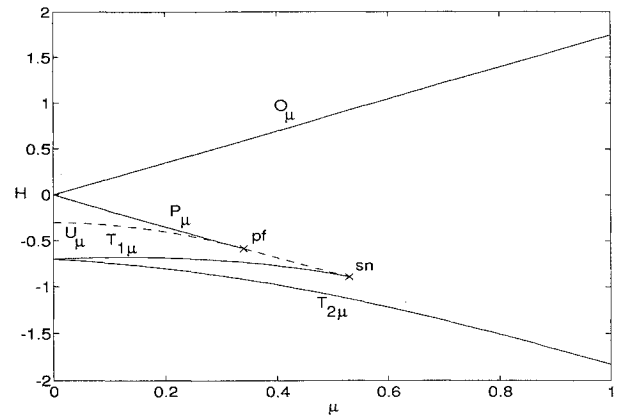

Fig. 5 μH plane for the oblate-prolate gyrostat.

Qualitatively, the three momentum spheres in Figs. 2–4 represent all of the possible momentum spheres for the gyrostat studied here, except for the spheres at the bifurcation values of μ. However, to show spin-up trajectories using momentum spheres, one must construct several spheres to illustrate the quasistatic progress of the spin-up trajectory and the instantaneous constant energy curves on the sphere. An alternative to viewing spin-up trajectories on momentum spheres is to use a single plane whose axes are the platform axial angular momentum μ and the system energy H.

The μH plane in Fig. 5 is a bifurcation diagram that shows the evolution of the energy H for the stable and unstable equilibria on the momentum sphere as μ varies. Solid lines represent centers and dashed lines represent saddles. The dashed line labeled U_μ represents two saddles that have the same energy. One sphere for a particular value of μ can be mapped to a corresponding vertical slice of the plane at that value of μ. Each closed orbit on a momentum sphere corresponds to a single point in the μH plane. Furthermore, a particular spin-up trajectory, which covers a range of μ, may be superimposed on this plane so that spin-up dynamics can be easily observed with respect to the equilibria. The lost information in this projection is the rapidly varying phase, denoted ϕ, which is discussed in more detail later. Thus for initial values of μ and H, there are infinitely many initial conditions corresponding to different initial phases.

The branches of equilibria in the μH plane depend on the spacecraft geometry. An unbalanced gyrostat of the class considered here corresponds to one of three general types.[6,7] These are termed oblate-prolate, oblate-intermediate, and intermediate-prolate depending on whether the plane containing the imbalance has the maximum and minimum, maximum and intermediate, or intermediate and minimum eigenvalues of $\boldsymbol{J}$, respectively. The definitions are summarized in Table 1, where we assume without loss of generality that $J_1 > J_3$. The analysis in this paper is limited to the oblate-prolate geometry. The μH plane in Fig. 5 has the same qualitative features as all gyrostats of this type. The other two types are discussed in more detail in Ref. 7.

Resonance Capture in Spin-up

Our approach uses projection of spin-up trajectories onto the μH plane, which has been rigorously justified using averaging and the

$\varepsilon = 0$ solution.[11,12] Spin-up trajectories typically begin near an all-spun equilibrium; i.e., the platform and rotor rotate together as a single body. It is straightforward to show that the all-spun condition is[12]

$$\mu_{as} = I_s \boldsymbol{a}^T \boldsymbol{I}^{-1} \boldsymbol{x} \tag{23}$$

That is, the all-spun platform angular momentum is I_s times the component of the angular velocity in the $\boldsymbol{a}$ direction. However, it is conceivable that spin-up could begin from any initial condition, and as shown later, the outcome of the maneuver is sensitively dependent on the initial conditions. Thus, we will consider spin-up from a large set of initial conditions based on initial platform momentum μ_0, initial energy H_0, and initial phase ϕ_0, which is defined later. We assume that spin-up concludes when the platform has completely despun ($\mu_f = 0$). Note that this implies the axial angular velocity of the platform is zero, but the transverse angular velocities will, in general, be nonzero due to the internal transverse constraint torques.

There are three types of spin-up trajectories for the oblate-prolate gyrostat. These are oblate spin-up, prolate spin-up, and resonance capture. The third condition has already been discussed and is the main topic of this section. Oblate and prolate spin-up as defined herein refer to the condition in which the spacecraft finally rotates about either the oblate (O_μ) or prolate (P_μ) equilibrium point. In the μH plane, these spin-up trajectories follow the respective equilibrium curves. Both of these spin-up conditions lead to escape.

Reference 5 shows how capture of an axial gyrostat is represented on a sequence of momentum spheres and in the μH plane. This can be easily extended to the spacecraft geometry studied here. If the final energy of the system (at $\mu_f = 0$) forms a closed curve about either of the transverse (or flat spin) equilibria, the trajectory has been captured. If this curve encircles either dual-spin center, then it has escaped. The set of all constant energy curves that surround a particular center are in its domain. These domains are isolated from one another by the separatrices. Moreover, because each closed curve within a given domain represents a specific rotational kinetic energy, we may specify the energy range of that domain.

A schematic representation is shown in Fig. 6, which depicts the four (numbered) domains at $\mu = 0$. The energy ranges are shown in the μH plane. They are shown at different values of μ for clarity. It is important to emphasize that for $\mu = 0$ all of these energies are defined and the energy ranges overlap; i.e., ranges 1 and 2 and ranges 3 and 4 overlap. The lower diagram in Fig. 6 is a two-dimensional representation of the momentum sphere for $\mu = 0$, showing only the equilibrium points and the separatrices. The momentum sphere is punctured at the equilibrium point O_μ [$\boldsymbol{x} = (0, 0, -1)$]. The resulting flattened sphere has five equilibria, and the edge is identified with the sixth equilibrium, namely O_μ. The two saddles (U_μ) are connected by the four separatrices that separate the numbered domains of the stable equilibria (O_μ, P_μ, $T_{1\mu}$, $T_{2\mu}$).

Notice that we define escape as a final rotation about either P_μ or O_μ. For $\mu = 0$, the domains of these two equilibria have the same energy range but correspond to different motions of the spacecraft. A more precise distinction could be drawn between the two escape conditions, but it could not be given in terms of the final energy. Thus we proceed with the given definition, pointing out where the distinction between P_μ and O_μ is relevant.

At the end of spin-up, the value of the final system energy H_f must lie in one of the energy ranges shown in Fig. 6. Taking Eq. (19) with $\mu = 0$, the final energy is

$$H_f = -\left(i_1 x_1^2 + i_2 x_2^2\right) \tag{24}$$

For $\mu = 0$, the equilibria correspond to steady rotation about one of the $\hat{p}_i$, and the saddle equilibria correspond to $x_2 = \pm 1$. Thus, we define the energy range of each domain in terms of the geometric parameters of the spacecraft:

Dual-spin energy range: $-i_2 < H_f < 0$

Transverse spin energy range: $-i_1 < H_f < -i_2$

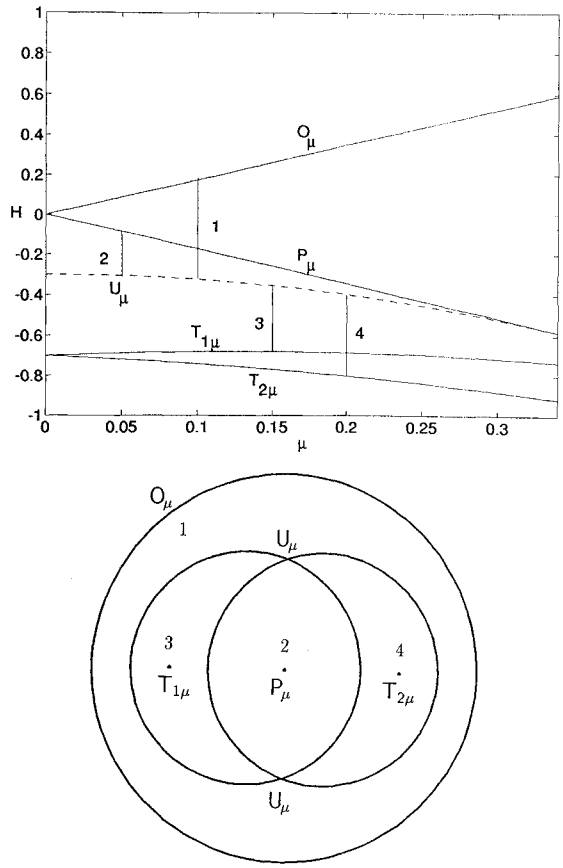

Fig. 6 Energy ranges at the end of spin-up.

With this result, the conditions for capture and escape are clear. From our previous discussion:

$$\begin{aligned} &\text{Escape: } -i_2 < H_f < 0 \\ &\text{Capture: } -i_1 < H_f < -i_2 \end{aligned} \tag{25}$$

Simple expressions for the criteria leading to the possibility of resonance capture for a slightly asymmetric, balanced gyrostat are developed in Ref. 5. However, in that paper, the probability of capture was only considered for one initial condition in the μH plane, whereas in the present work we are interested in the probability of capture for essentially all initial conditions. Thus, except for the criteria developed earlier in Eqs. (25), our results are graphical in nature and are based on numerical integration of the equations of motion.

Referring to the μH plane as shown in Figs. 5 and 6, we note that spin-up trajectories projected onto the μH plane will flow from right to left since $\dot{\mu} = \varepsilon < 0$ for the class of problems considered here. Also, any trajectory will be roughly parallel to one of the solid curves of equilibria (O_μ, P_μ, $T_{1\mu}$, $T_{2\mu}$) depending on which of the unperturbed centers the trajectory is approximately oscillating about. Thus a trajectory that begins near $T_{2\mu}$ at, say, $\mu_0 = 0.6$, will follow $T_{2\mu}$ all of the way to the $\mu_f = 0$ final condition, resulting in capture. However, a trajectory that begins at $\mu_0 = 0.6$ and farther from $T_{2\mu}$ (larger H_0) may cross the dashed line of instantaneous separatrices connecting the pitchfork and saddle-node bifurcations. After that crossing it may remain near $T_{1\mu}$ (capture), or it may cross one of the U_μ separatrices to end up oscillating about P_μ (escape).

An important characteristic that distinguishes our spin-up model from the axial case[5] is the significance of separatrix crossing. Although a trajectory of the perturbed system must cross an instantaneous separatrix of the unperturbed system for capture of the balanced asymmetric gyrostat,[5] this is not necessarily true for the unbalanced model. By looking at the μH plane of a typical oblate-prolate gyrostat (Fig. 5), we see that the trajectories of the transverse equilibria ($T_{1\mu}$ and $T_{2\mu}$) form a pocket for $\mu < \mu_{sn}$. Spin-up

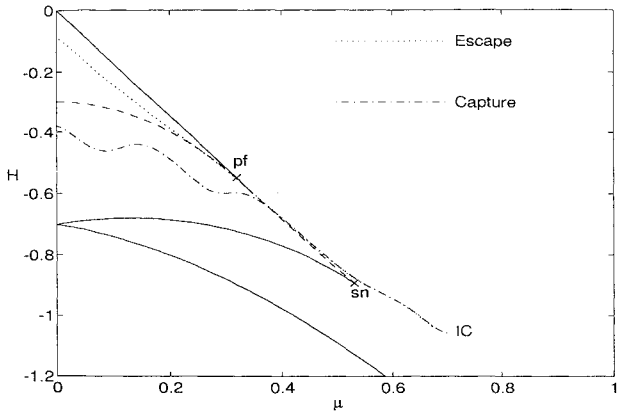

Fig. 7 Capture and escape resulting from two different initial conditions.

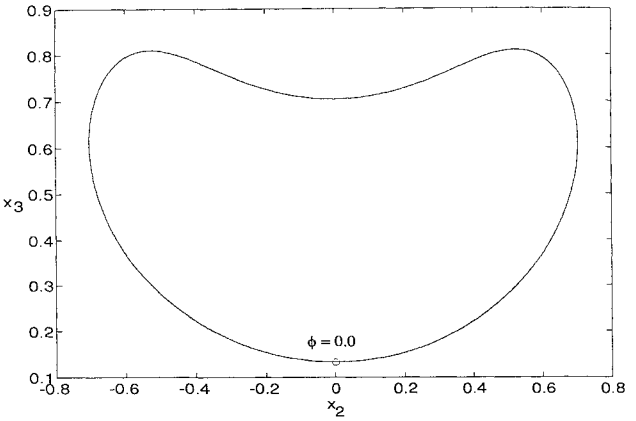

Fig. 8 Constant energy curve for $\mu = 0.7$ and $H = -1.0576$.

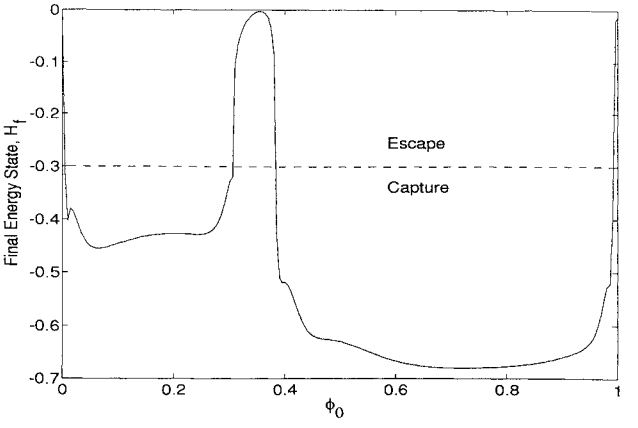

Fig. 9 Final energy vs initial phase ($\mu_0 = 0.7$ and $H_0 = -1.0576$).

trajectories that lie within this region have not crossed a dashed line in the μH plane, but they continue to oscillate about one of the transverse equilibria and are therefore captured. Taking this observation one step further, it can be seen that a separatrix crossing will in fact result in escape for initial conditions near $T_{1\mu}$ or $T_{2\mu}$ with $\mu_0 < \mu_{sn}$. The pitchfork bifurcation marks the transformation of P_μ from a saddle to a center, and so the trajectory that oscillates initially about either $T_{1\mu}$ or $T_{2\mu}$ must cross a separatrix to escape.

Effects of the Motor Torque ε

To eliminate the possibility of resonance capture during spin-up of prolate spacecraft, it has been shown that larger motor torques are required.[2,3,7] The cost of this alternative is the greater size and weight associated with a more powerful motor. Because of physical constraints, this may not be a viable solution. Reference 5 shows that a larger motor torque is not always necessary because the initial conditions also affect the likelihood of capture.

Effects of Initial Phase

For a given motor torque ε and initial conditions μ_0 and H_0 for which capture occurs, escape may still be possible. For example, in Fig. 7 we show two spin-up trajectories beginning at the same point in the μH plane but having distinctly different final conditions; specifically, one trajectory escapes, whereas the other is captured. This is achieved not with a larger spin-up motor but by choosing a different initial angular phase on the momentum sphere.

The angular phase ϕ is defined for $\varepsilon = 0$ and represents the position of the angular momentum vector on a given closed constant energy curve. If the period of a given curve is denoted by P, then $\phi = t/P$, where $t = 0$ at some arbitrary point on the curve; thus $\phi \in [0, 1)$. With this phase variable, we have effectively reduced the number of variables that define the system angular momentum from four (x_1, x_2, x_3, μ) to three (ϕ, μ, H). This reduction is discussed in detail in Refs. 11 and 12.

Resonance capture can be avoided by varying the initial phase ϕ_0. The curve in Fig. 8 shows the set of all possible initial conditions for the system angular momentum vector with $\mu_0 = 0.7$ and $H_0 = -1.0576$. This trajectory lies within the domain of $T_{2\mu}$ and represents an unperturbed ($\varepsilon = 0$) trajectory of the system just before spin-up. As ϕ undergoes a complete cycle, it follows the curve in a counterclockwise direction starting and ending at the point denoted by ○. During spin-up, the angular momentum vector is no longer constrained to this curve. Its path may take it away from $T_{2\mu}$ into the domain of P_μ (escape), or it may continue to oscillate about $T_{2\mu}$ (capture). The actual path depends on the initial phase.

To determine which of these initial conditions leads to capture and which to escape, the initial phase ϕ_0 is allowed to vary along this curve, and the final energy H_f is calculated for each initial condition. The resulting final energies plotted against their respective initial conditions from the constant energy curve of Fig. 8 are shown in Fig. 9. Application of Eqs. (25) determines which final energy states result in capture. Thus, capture occurs if $H_f < -i_2 = -0.3$.

It is evident from Fig. 9 that most of this particular set of initial conditions leads to capture and that the outcome of spin-up is especially sensitive to small changes in ϕ_0 for ϕ_0 near 0, 0.3, and 0.4. These particular values are in turn sensitive to changes in ε and the inertia parameters. This sensitivity is due to the fact that the trajectories cross an instantaneous separatrix of the unperturbed ($\varepsilon = 0$) system, as discussed in detail in Ref. 11. However, the curve in Fig. 9 is qualitatively correct for all values of the inertia parameters and for small values of the torque ε. The most important conclusion that can be drawn from this figure is that it is possible to choose initial conditions for which resonance capture does or does not occur. Hence one should avoid making decisions based solely on simulation results with a small sampling of initial conditions.

Probability of Capture

We now extend this idea to consider the probability of capture[13] for given initial conditions (μ_0, H_0). The probability of capture is denoted by P_c and is defined as the number of initial conditions leading to capture divided by the total number of initial conditions for the given initial values of μ and H. Computation of P_c for a given initial point in the μH plane involves numerically integrating the equations of motion for a large number, say N_0, of initial values of the phase $\phi_0 \in [0, 1)$. For each trajectory, the final energy H_f determines whether capture or escape occurs. Letting N_c be the number of trajectories that are captured, the probability of capture is simply

$$P_c = N_c/N_0 \tag{26}$$

Graphically, since $\phi_0 \in [0, 1)$, P_c is simply the length of the intervals of ϕ_0 for which the final energy state $H_f < -i_2$. For example, $P_c = 0.9064$ for the initial energy curve in Fig. 8, as calculated using Fig. 9.

The probability of capture has been found for a single initial constant energy curve ($H_0 = -1.0576$) on a particular initial momentum sphere ($\mu_0 = 0.7$). Our next step is to extend this calculation

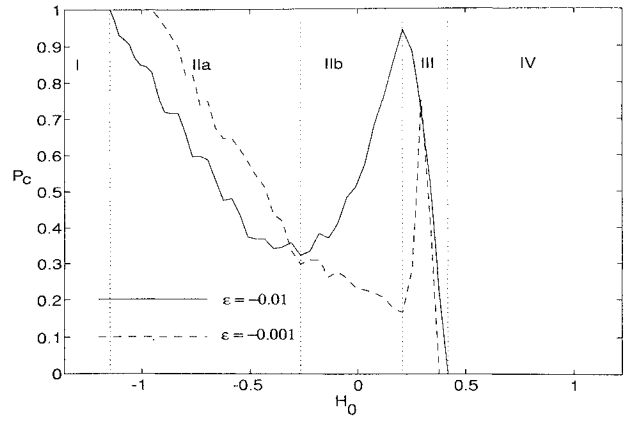

Fig. 10 Probability of capture vs initial energy at $\mu_0 = 0.7$.

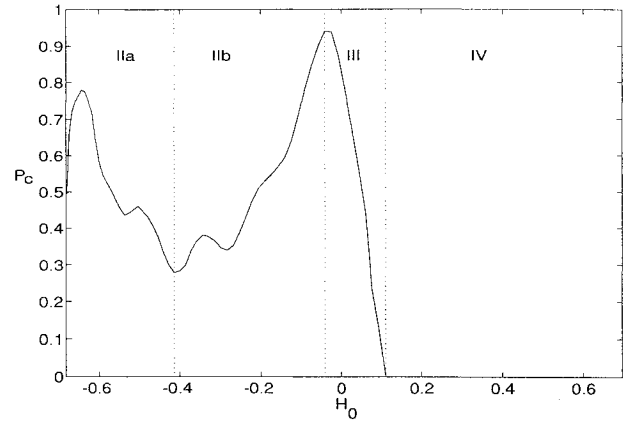

Fig. 11 Probabilities of capture in the domain of O_μ ($\mu_0 = 0.4$).

to all possible constant energy curves on a given sphere. This corresponds to finding P_c at different points along a particular vertical slice of the μH plane. Then the calculation is extended over the entire μH plane to obtain P_c for different momentum spheres. In effect, we determine the probabilities of capture for a grid of initial conditions on the μH plane.

The μH plane can be divided into three distinct regions depending on the number of equilibria in each (cf. Figs. 2–5). Region A has six equilibria and four subregions (1–4) (cf. Fig. 6). The part of the μH plane to the left of μ_{pf} belongs to this region. Region B has four equilibria and three subregions (5–7) and covers the portion of the μH plane between μ_{pf} and μ_{sn}. Region C has two equilibria and no subregions and covers the remainder of the μH plane. Each subregion corresponds to the domain of a stable equilibrium point on the momentum sphere. The determination of P_c in each region is discussed individually.

First we examine the probabilities of capture for initial conditions in region C. The term P_c for a single point in this region has already been determined earlier. We now perform the same calculation at the same initial value of μ_0 (0.7 in our example) but over the entire range of H_0. Each initial energy corresponds to a closed curve around a center. As can be seen from Fig. 4, there are no separate domains in this region. Hence, H_0 can take any value between the energies associated with O_μ and P_μ. By plotting P_c against this range of initial energies, we obtain the solid curve in Fig. 10, which has some interesting properties. This figure shows four distinct areas of interest, labeled by the corresponding Roman numerals. Note that area II has been divided into two subareas.

Area I is a region of guaranteed capture, i.e., $P_c = 1$. For $\varepsilon = -0.01$, $\mu_0 = 0.7$, and $-1.50 \leq H_0 \leq -1.15$, all initial conditions lead to capture. Area IV ($0.42 \leq H_0 \leq 1.22$) is a region of guaranteed escape. Unlike areas I and IV, areas II and III have diverse probabilities. If spin-up is initiated in either of these areas, capture may or may not occur. In area II ($-1.15 \leq H_0 \leq 0.24$), P_c is a roughly parabolic function of H_0. In this interval, P_c has a local minimum (in this case at $H_0 = -0.27$). A local maximum at $H_0 = 0.24$ separates areas II and III.

As an interesting aside, we compare the overall probabilities of capture for two identical spacecraft with different motor torques. By superimposing a (dashed) curve for $\varepsilon = -0.001$, the composite plot of Fig. 10 results. From this picture, we can see that spacecraft that undergo prolate spin-up (low values of H_0) have a better chance to escape if a larger motor is used, as has been documented throughout the literature. If, however, oblate spin-up is desired (higher values of H_0), a smaller motor torque has a slightly better performance. More importantly, the qualitative features of P_c vs H_0 are unaffected by the change in torque. Thus our approach is useful even in the presence of unavoidable parameter uncertainties.

Region B

Calculation of P_c for initial conditions in this region is more involved. Because there are three domains, the procedure must be repeated three times. We compute the probabilities of capture at initial conditions that lie within each domain, thereby obtaining for each case a plot similar to Fig. 10. Note that in region C no separatrices delimit the domains of the oblate and prolate equilibrium points; hence, the entire region is a single domain. In region B (and in A), the stable centers are separated by the separatrices (cf. Figs. 2 and 3). The range of initial energy curves in each domain, when viewed on the momentum sphere, covers the entire domain from the stable center up to and including the separatrix.

The probabilities of capture for initial conditions in the domain of O_μ are shown in Fig. 11. Note the similarity to Fig. 10 and that there is no area I; i.e., there is no region of guaranteed capture. The term P_c is unity throughout most of the transverse spin domains (not shown). Since these domains grow during spin-up, trajectories that begin near a transverse center will continue to circle these equilibria at motor shutoff. Initial conditions very close to the separatrices, however, may cross into the domain of P_μ. Thus the transverse spin domains are analogous to area I as previously described for region C, with some area IIa behavior for trajectories beginning near a separatrix.

Region A

Region A has four domains (cf. Fig. 6). The same procedure is used to determine the probabilities of capture. Again, the domains of $T_{1\mu}$ and $T_{2\mu}$ predominantly exhibit area I behavior, but this time with area IIa behavior as well. Of greater interest are the domains of O_μ and P_μ. Within the domain of O_μ, the region of negative slope characteristic of area IIa is truncated, leaving only the steep ascent and peak of IIb. The equally dramatic drop and the region of guaranteed escape that characterize areas III and IV remain qualitatively unchanged. The spin-up behavior for initial conditions within the domain of P_μ, nonexistent for regions B and C, is even more intriguing. In this domain, the probability of capture is zero throughout. The reason for this is that the P_μ domain grows with time. Hence, trajectories that start near P_μ will remain near P_μ.

Probabilities of Capture Throughout the μH Plane

Now that we have seen how the overall probabilities of capture vary on the three distinct momentum spheres that characterize the oblate-prolate gyrostat, the results obtained earlier can be transcribed onto the μH plane. The probabilities of capture for initial conditions within any single stable equilibrium domain, as well as any combination of these domains, can be shown over the entire range of μ. The major areas that depict important trends in P_c, similar to those described in Fig. 10, are marked on this plot to locate favorable and unfavorable initial conditions. It must be emphasized, however, that this is only useful if combinations of equilibria whose domains do not overlap on the μH plane are considered, such as $T_{1\mu}$–P_μ or $T_{2\mu}$–O_μ. Figure 12 depicts the probabilities of capture for initial conditions in the $T_{2\mu}$ and O_μ domains for all values of μ. Areas I–IV, as previously described, are labeled.

Diagrams such as Fig. 12 are useful tools for spacecraft designers and operators. They can be considered maps from which the best initial condition for spin-up is chosen to avoid resonance capture. Area I must be avoided and area IV is ideal. However, given the constraints of spacecraft geometry and available power,

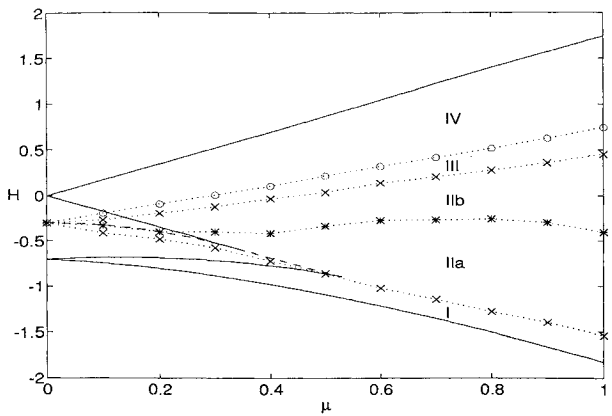

Fig. 12 Probabilities of capture for initial conditions throughout the μH plane.

jockeying the satellite into area IV before spin-up may not be feasible. More realistically, the designer could use such a map to obtain qualitative information about the probability of capture for different spacecraft designs. If used in conjunction with plots similar to Fig. 10, the likelihood of a successful spacecraft attitude acquisition is maximized.

Conclusions

We have established fundamental criteria for resonance capture and have shown how different conditions affect the probability of capture. It has been shown in the literature that large motor torque provides a better likelihood for escape than small torque. For a given motor torque, whether resonance capture occurs or not is also sensitively dependent on the initial conditions. For given initial values of the platform momentum μ and system energy H, initial conditions lie on a closed curve on the surface of the momentum sphere that may be parameterized by an initial angular phase ϕ_0. By varying ϕ_0, the probability of capture may be determined for initial conditions on this curve. Repeating this procedure throughout the domains of the stable centers, and making use of the μH plane, results in a simple map that shows qualitatively which initial conditions have the greatest and least probability of capture.

References

[1]Scher, M. P., and Farrenkopf, R. L., "Dynamic Trap States of Dual-Spin Spacecraft," *AIAA Journal*, Vol. 12, No. 12, 1974, pp. 1721–1724.

[2]Kinsey, R. J., "Despin of a Dual-Spin Spacecraft with Limited Torque: Passage Through Precession Phase Lock Resonance," Ph.D. Dissertation, Mechanical, Aerospace and Nuclear Engineering Dept., School of Engineering and Applied Science, Univ. of California, Los Angeles, CA, 1991.

[3]Kinsey, R. J., Mingori, D. L., and Rand, R. H., "Spinup Through Resonance of Rotating Unbalanced Systems with Limited Torque," *Proceedings of the 1990 AIAA/AAS Astrodynamics Conference*, Pt. 2, AIAA, Washington, DC, 1990, pp. 805–813.

[4]Or, A. C., "Resonances in the Despin Dynamics of Dual-Spin Spacecraft," *Journal of Guidance, Control, and Dynamics*, Vol. 14, No. 2, 1991, pp. 321–329.

[5]Hall, C. D., "Resonance Capture in Axial Gyrostats," *Journal of the Astronautical Sciences* (to be published).

[6]Hall, C. D., "Spinup Dynamics of Biaxial Gyrostats," *Journal of the Astronautical Sciences* (to be published).

[7]Tsui, R., "Resonance Capture in Unbalanced Dual-Spin Spacecraft," M.S. Thesis, Graduate School of Engineering, Air Force Inst. of Technology, Wright–Patterson AFB, OH, March 1994.

[8]Hughes, P. C., *Spacecraft Attitude Dynamics*, Wiley, New York, 1986, Chap. 5.

[9]Barba, P. M., and Aubrun, J. N., "Satellite Attitude Acquisition by Momentum Transfer," *AIAA Journal*, Vol. 14, No. 10, 1976, pp. 1382–1386.

[10]Hubert, C. H., "Dynamics of the Generalized Dual-Spin Turn," *RCA Review*, Vol. 41, No. 3, 1980, pp. 449–471.

[11]Hall, C. D., and Rand, R. H., "Spinup Dynamics of Axial Dual-Spin Spacecraft," *Journal of Guidance, Control, and Dynamics*, Vol. 17, No. 1, 1994, pp. 30–37.

[12]Hall, C. D., "Spinup Dynamics of Gyrostats," *Journal of Guidance, Control, and Dynamics* Vol. 18, No. 5, 1995, pp. 1177–1183.

[13]Henrard, J., "Capture Into Resonance: An Extension of the Use of Adiabatic Invariants," *Celestial Mechanics*, Vol. 27, No. 1, 1982, pp. 3–22.